doi:10.1016/j.jmb.2011.12.049 J. Mol. Biol. (2012) 417, 51–64

Contents lists available at www.sciencedirect.com

Journal of Molecular Biology

journal homepage: http://ees.elsevier.com.jmb

The C-Terminal Tail of Human Neuronal Calcium Sensor 1 Regulates the Conformational Stability of the Ca^{2+}-Activated State

Pétur O. Heidarsson[1], Ida J. Bjerrum-Bohr[1], Gitte A. Jensen[1], Olaf Pongs[2], Bryan E. Finn[3], Flemming M. Poulsen[1]† and Birthe B. Kragelund[1]*

[1]*Structural Biology and NMR Laboratory, Department of Biology, University of Copenhagen, Ole Maaløes Vej 5, DK-2200 Copenhagen, Denmark*
[2]*Institute for Neural Signal Transduction, University Medical Center, Hamburg-Eppendorf, Martinistrasse 52, D-20246 Hamburg, Germany*
[3]*Swedish University of Agricultural Sciences, Box 35, 230 53 Alnarp, Sweden*

Received 7 November 2011; received in revised form 19 December 2011; accepted 23 December 2011
Available online 29 December 2011

Edited by M. F. Summers

Keywords:
NCS-1;
NMR;
membrane interaction;
calcium binding;
protein stability

Neuronal calcium sensor 1 (NCS-1) and orthologs are expressed in all organisms from yeast to humans. In the latter, NCS-1 plays an important role in neurotransmitter release and interacts with a plethora of binding partners mostly through a large solvent-exposed hydrophobic crevice. The structural basis behind the multispecific binding profile is not understood. To begin to address this, we applied NMR spectroscopy to determine the solution structure of calcium-bound human NCS-1. The structure in solution demonstrates interdomain flexibility and, in the absence of a binding partner, the C-terminal tail residues occupy the hydrophobic crevice as a ligand mimic. A variant with a C-terminal tail deletion shows lack of a defined structure but maintained cooperative unfolding and dramatically reduced global stability. The results suggest that the C-terminal tail is important for regulating the conformational stability of the Ca^{2+}-activated state. Furthermore, a single amino acid mutation that was recently diagnosed in a patient with autistic spectrum disorder was seen to affect the C-terminal tail and binding crevice in NCS-1.

Introduction

Neuronal calcium sensor 1 (NCS-1) is a 190-residue (22 kDa) N-terminally myristoylated EF-hand protein that is involved in the efficient transduction of nerve stimuli in synaptic nerve endings, where it potentiates neurotransmitter release.[1–3] It belongs to the NCS family, a subfamily of the larger EF-hand calcium binding protein family that shares a structural scaffold of four EF hands coordinating two or three calcium ions.[4] EF hands always occur in pairs called an EF-domain.[5] In the NCS family, two domains are defined: the N-domain, which consists of EF1 and

*Corresponding author. E-mail address: bbk@bio.ku.dk.
Present address: I. J. Bjerrum-Bohr, Department of Food Science, Faculty of Life, University of Copenhagen, DK-2200 Copenhagen, Denmark.

† We honor the memory of F. M. Poulsen, who died during the preparation of this article.

Abbreviations used: NCS-1, neuronal calcium sensor 1; 3D, three-dimensional; HC, hydrophobic crevice; NOESY, nuclear Overhauser enhancement spectroscopy; HSQC, heteronuclear single-quantum coherence; TOCSY, total correlated spectroscopy; NOE, nuclear Overhauser enhancement; GuHCl, guanidine hydrochloride; 2D, two-dimensional.

EF2, and the C-domain, which consists of EF3 and EF4. A few three-dimensional (3D) structures for NCS-1, determined by either X-ray crystallography or NMR spectroscopy, are available. Based on NMR restraints and homology modeling, the earliest structure solved was that of budding yeast Frq1 (*Saccharomyces cerevisiae*), an orthologue of human NCS-1,[6] followed by the crystal structure of human NCS-1.[7] The crystal structure of NCS-1 in its calcium-loaded nonmyristoylated state forms an elongated flat shape with a hydrophobic crevice (HC) on one side of the structure opposite the calcium ions. In this structure, the crevice is occupied by adjuvant molecules of polyethylene glycol. Three of the four EF hands in NCS-1 (EF2, EF3, and EF4) bind Ca^{2+}, while EF1 is unable to do so due to a conserved Cys/Pro substitution in the calcium binding motif. EF2 and EF3 have been identified as structural sites, being occupied by Mg^{2+} in the absence of Ca^{2+}, while EF4 is regarded as a sensory site, binding only Ca^{2+} and with lower affinity.[8] Without calcium and magnesium, the apo state lacks a stably folded core, and binding of Ca^{2+} leads to stabilization and a large conformational change into a binding-competent state that allows for interactions with a vast array of interaction partners.[6] Since little structural information on the Ca^{2+}-free state is available, the exact nature of the structural change is not clear. NMR studies indicate that the apo state has the characteristics of a molten globule, showing resonance signals only for a subset of residues, or it may form multimeric species, leading in both cases to broadened NMR signals.[6] It should be noted that the apo state of NCS-1 likely exists only transiently *in vivo*, since background magnesium levels in cells are high. The magnesium-bound state apparently also exists in a molten-globule-like state, yet with more structure than the apo form.[8] The Ca^{2+}-free myristoylated form of Ncs1 from fission yeast *Schizosaccharomyces pombe* does, however, have a well-defined structure as demonstrated recently,[9] emphasizing the significant degree of structural differences between yeast Ncs1 and mammalian NCS-1 despite a 59% sequence identity between them.[4]

The N-terminal glycine is myristoylated *in vivo* through the action of *N*-myristoyltransferase, enabling NCS-1 to dock onto the membrane, and reports have suggested that NCS-1 is constitutively bound to the membrane in a calcium-dependent manner.[10] The functional mechanism of membrane docking via the lipid has been debated, mostly in light of the calcium–myristoyl conformational switch that has been so clearly described for its related family member, recoverin.[11–13] A newly reported structure of myristoylated fission yeast Ncs1 suggests the existence of different modes for packing the myristoyl group, supporting the view of structural heterogeneity in the NCS proteins.[9] The data suggest that the yeast homolog possesses an alternative calcium–myristoyl switch to recoverin. Whether this is also the case for mammalian NCS-1 remains to be established.

Numerous interaction partners have been suggested. The first interaction partner to be described was the phosphatidylinositol 4-kinase Pik.[14] The structure of yeast Frq1, in complex with an N-terminal Pik1 fragment ($Pik1^{121–174}$), has been solved and shows that the peptide binds into the HC of Frq1 with the C-terminal tail of Frq1 at the edge of the groove.[15] Other reported interaction partners include G-protein-coupled receptor kinase (GRK2),[16] dopamine D2 receptor,[17] Kv4.2 potassium channel,[18] IL1RAPL (*IL-1 r*eceptor *a*ccessory *p*rotein *l*ike) protein,[19] calcineurin,[20] and the calmodulin-dependent cyclic nucleotide 3′,5′-phosphodiesterase.[20] How this polymorphous and rather multispecific binding profile agrees with a highly folded and globular protein has never been addressed, and structures of more complexes need to be available to draw more general conclusions. Nevertheless, in this respect, the HC of NCS-1 emerges as a striking feature due to its solvent accessibility, which is evident from the crystal structures, and to the location of the Pik1 binding site. Likewise, protein flexibility may play a role in ligand binding, as evidenced by the conformational adaptation in binding that has been amply described for another EF-hand protein, calmodulin.[21]

To obtain a mammalian NCS-1 scaffold in solution that would allow us to dissect structural features with a focus on the crevice, we solved the solution structure of human NCS-1 using NMR spectroscopy. In conjunction with structural alignments using previous NCS-1 structures and mutational studies, a key role for the last 15 residues forming a C-terminal tail emerges, acting as an aegis to the crevice, where it regulates conformational stability and, presumably, ligand binding. In addition, a mutation that leads to structural and functional deficits has effects on the aegis, and we speculate on the possible pathological consequences of this.

Results

NMR solution structure of human NCS-1

From a set of triple-resonance heteronuclear NMR spectra, backbone resonance assignments for 175 of the 190 residues could be obtained.[22] Assignments could not be obtained for the first five residues in the N-terminus and for 10 other residues, of which seven were prolines. From ^{13}C nuclear Overhauser enhancement spectroscopy (NOESY) heteronuclear single-quantum coherence (HSQC) and HCCH total correlated spectroscopy (TOCSY) spectra, side-chain

resonances were partially or fully assigned for all residues, including the prolines, except for the first five residues in the N-terminus, which were completely absent from all spectra, as well as for L97 and K147, where backbone and C^{β} of the side chain only could be assigned. Despite extensive overlap in the aromatic region including 15 phenylalanines, 12 of which are located in the N-domain, side-chain assignments were achieved for 12 phenylalanines, all 7 tyrosines, and both tryptophans. This pattern is similar to the NMR assignments of previous studies on NCS-1/Frq1.[6] From chemical shift assignments and using TALOS,[23] we derived 248 dihedral-angle restraints. From the NOESY spectra, a total of 1297 ^{1}H–^{1}H nuclear Overhauser enhancements (NOEs) with useful distance information were obtained, resulting in a sparse number of only ~7 restraints per residue. Calcium coordination was included according to the procedure previously described,[24] adding another 18 restraints. Based on $^{3}J_{HN-H\alpha}$ coupling constants, chemical shifts, amide hydrogen exchange, NOE patterns, and structure evaluations, 63 hydrogen-bond restraints were added in secondary structures.

The solution structure of human NCS-1 at pH 7.2 and 37 °C was solved based on a total of 1626 restraints (Table 1). A final set of 100 structures was calculated using Xplor-NIH,[25] and the 20 structures with the lowest energy were selected to represent the structure (Fig. 1a). None of these had restraint violations larger than 0.5 Å (NOEs) and 5° (dihedral angles). Compared to the size of NCS-1, the number of NOEs was low and not evenly distributed. Especially in the N-domain and particularly in the first two helices, a lower number of NOEs were assigned.

The final structure consisted of nine α-helices as follows: helix H1 (E11-R18), helix H2 (E24-F34), helix H3 (A45-Q54), helix H4 (T62-F72), helix H5 (F82-S93), helix H6 (D98-Y108), helix H7 (R118-V132), helix H8 (Q146-M155), and helix H9 (L166-K174), in which helices H2–H9 are arranged in the four classical EF hands (Fig. 1b). The extent of the helices was defined from a combination of information derived from sequential and medium-range NOE cross-peaks, $^{3}J_{HN-H\alpha}$ coupling constants, slow amide proton exchange, secondary chemical shift values, and inspection of the structures. A 10th helix, which has been observed in the crystal structure of human NCS-1 and in the NMR structure of yeast Frq1 in complex with Pik1, and which involves the C-terminal residues S178-S184, was not identified in our data from the patterns of NOEs or from chemical shifts.[22] Six regions with three or more consecutive residues in β-type conformation were present in the structure. These are β1 (Q42-D44), β2 (F58-D60), β3 (R79-V81), β4 (Y115-T117), β5 (V136-L138), and β6 (K163-T165). Four of these (β1, β3, β4, and β6) are located in between helices in the calcium binding loops. Three loops were observed in the structure consisting of residues F56-P61 (L1), G133-P145 (L2), and D176-V190 (L3).

The eight helices H2–H9 shape together an HC, of which helices H4, H5, and H6 contribute to the floor of the crevice, helices H3 and H7 (on one side) and helix H9 (on the other side) contribute to the walls, and helices H8 and H2 form the ends, respectively (Fig. 1c). The peptide backbones of the 20 structures superimpose with a root-mean-square deviation (RMSD) of 1.9 ± 0.5 Å for the entire backbone (S6-V190), a backbone RMSD of 1.2 ± 0.3 Å for the first two EF hands (S6-G95), and a backbone RMSD of

Table 1. Summary of experimental restraints and structural statistics for the NMR solution structure of NCS-1

Experimental restraints	
Distance restraints	
Total	1297
Intraresidue	157
Sequential	426
Medium range	395
Long range	319
Dihedral-angle restraints, total	248
Φ	124
Ψ	124
Hydrogen-bond restraints	63
Calcium coordination restraints	18
Total number of restraints	1626
Restraint violations	
NOE violations > 0.3 Å	8
NOE RMSD (Å)	0.028 ± 0.002
Dihedral-angle violations > 5°	0
Dihedral-angle RMSD	0.014 ± 0.006
Deviation from ideal geometry (RMSD)	
Impropers (°)	0.242 ± 0.006
Bonds (Å)	0.00201 ± 0.00005
Angles (°)	0.297 ± 0.006
Energies (kcal mol^{-1})	
Total	−1870 ± 80
Bond	12.6 ± 0.7
Angle	74 ± 3
Impropers	14.4 ± 0.8
Van der Waals	−500 ± 20
Electrostatics	−1520 ± 80
NOE restraint	48 ± 8
RMSD of atomic positions (Å)[a]	
Backbone atoms[b]	1.17/1.80/1.93/1.50
All heavy atoms[c]	1.68/2.34/2.36/2.02
Ramachandran plot (%)	
Most favored regions	84.8
Additionally allowed regions	10.7
Generously allowed regions	3.5
Disallowed regions	1.0

[a] Calculated using iCING (http://nmr.cmbi.ru.nl/icing/iCing.html#file).
[b] Calculated as RMSD from the first structure for residues Ser6-Gly95, Thr96-Val190, Ser6-Val190, and Ser6-A175.
[c] Calculated as RMSD from the first structure for residues Ser6-Gly95, Thr96-Val190, Ser6-Val190, and Ser6-A175.

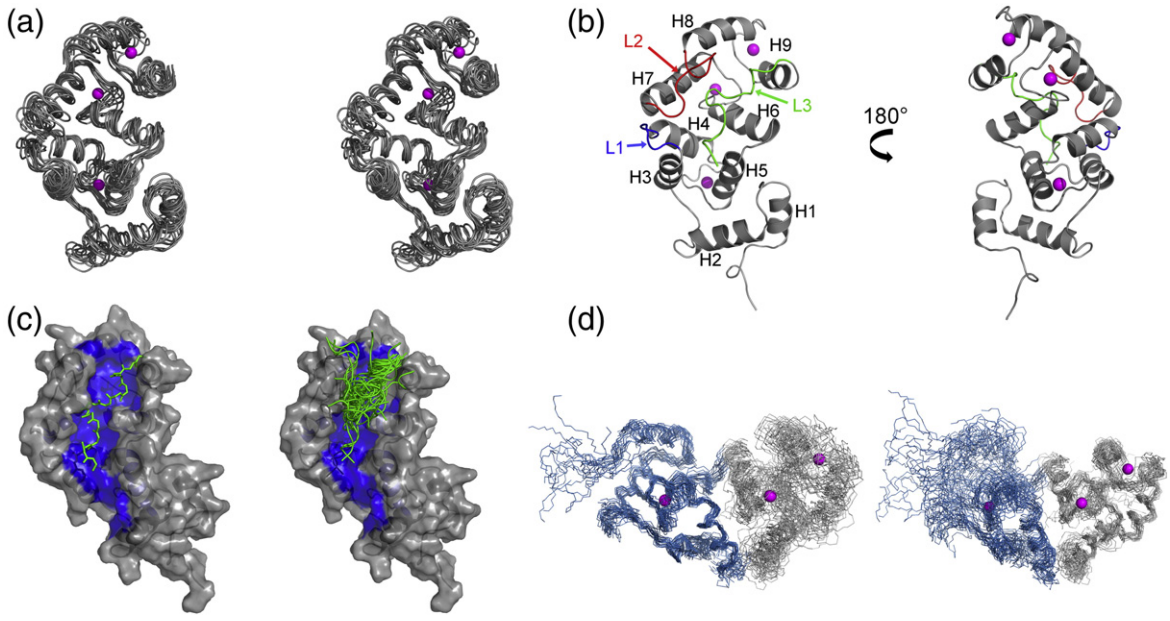

Fig. 1. The solution structure of Ca^{2+}-bound unmyristoylated human NCS-1. (a) Backbone alignment of 10 of the 20 lowest-energy structures, in stereo view. The L2 and L3 regions have been omitted for clarity. The structures were aligned in regions with secondary structures. (b) Cartoon representation of the NMR structure of NCS-1 illustrating the positions of helices H1–H9 (gray) and loops L1, L2, and L3 (blue, red, and green, respectively). The Ca ions bound in the EF2, EF3, and EF4 structural motifs are shown as spheres in magenta, where the bottom ion is bound to EF2, the middle ion is bound to EF3, and the top ion is bound to EF4. (c) L3 and the HC. Left: The lowest-energy structure of NCS-1 in space-filled surface representation and the main chain of L3 consisting of the C-terminal tail residues D176-V190 (green sticks). Right: The lowest-energy structure of NCS-1 with the 20 lowest-energy L3 structures superimposed. The residues in blue are hydrophobic residues of the HC. (d) Backbone alignment of the 20 lowest-energy structures of NCS-1 using separate domains. Alignment of helices H2–H5 (left) and H6–H9 (right).

1.8 ± 0.4 Å for the last two EF hands (T96-V190). Without L3 (S6-A175), the RMSD is 1.5 ± 0.4 Å. This suggests that the relative orientation of the two EF-domains cannot be defined by the data indicating mobility between the two parts of the structure (Fig. 1d) and mobility of L3 relative to the protein scaffold. It may also explain in part the low number of observed NOEs.

Several NOEs between the hydrophobic residues of the C-terminal L3 and the residues from helices H6, H7, and H9 were observed. Especially residues I179, V180, A182, and L183 were within 5 Å of the residues A104, I128, N143, T144, M155, M156, F169, and S173. The outermost seven residues (S184-V190) did not have any NOE contacts with the remainder of the protein and are thus not well defined in the structure.

Different interaction patterns between L3 and HC among NCS-1 structures

Previously, a number of NCS-1 structures in the Ca^{2+}-bound state have been solved: one crystal structure of human NCS-1 and three NMR structures of yeast homologues. Of the NMR structures, one is a structure of the free protein, two are in complex with a Pik1 peptide fragment, and the coordinates of the most recent are not available.[6,7,9,15] In addition, the structure of the Ca^{2+}-free myristoylated fission yeast Ncs1 has been determined by NMR.[9] In the crystal structure, several hydrophobic adjuvants are trapped in the HC and may stabilize a particular conformation. In the NMR structure of the yeast complex, the HC is clearly occupied by the Pik1 peptide; in that of the unbound state, NOEs used to define the N-domain were adapted from the unbound state of recoverin.[6] In the Ca^{2+}-free myristoylated form, it appears that the myristoyl group occupies the C-terminal part of the HC, in contrast to recoverin, where the myristoyl group has been shown to be embedded in the N-domain.[9]

We compared the human NCS-1 NMR solution structure to the three available Ca^{2+}-bound structures from the Protein Data Bank using Modeller,[26] counting the number of C^{α} atoms within 2 Å (Fig. 2a, Table 2) and matching the present NOE set to the one used for the structure determination of calcium-loaded unbound NCS-1 from yeast (Fig. S1). It is immediately apparent that the crystal structure of NCS-1 is more similar to the NMR structure of NCS-1 in complex with $Pik1^{121–174}$, which is not surprising given the occupancy by small hydrophobic

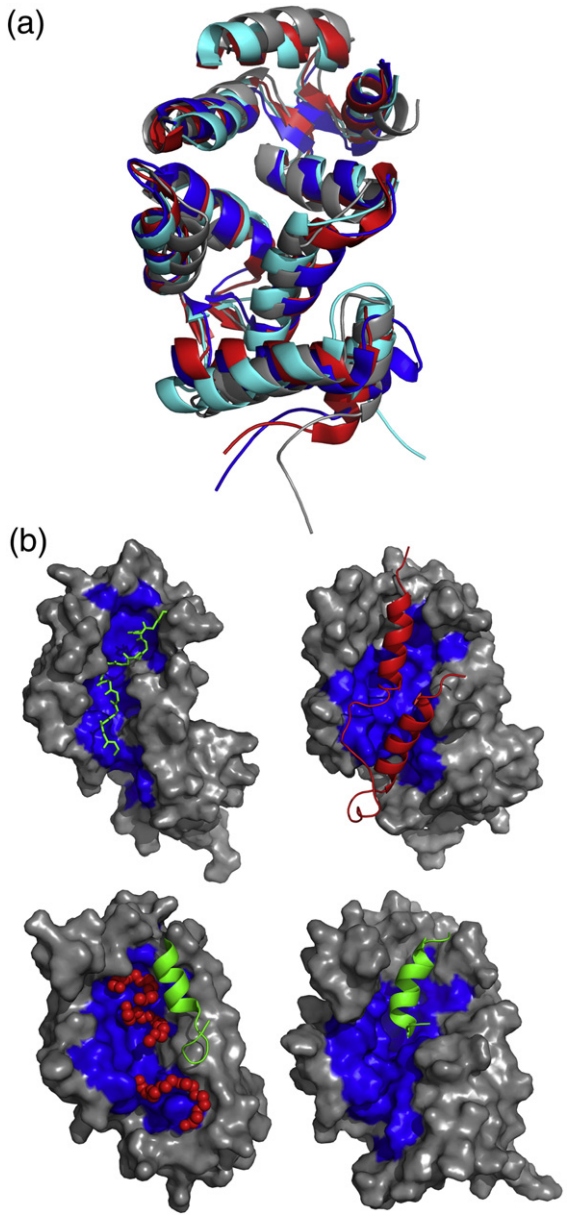

Fig. 2. Comparison of the human NCS-1 NMR solution structure to other available Ca^{2+}-loaded NCS-1 structures. (a) Backbone alignment of the lowest-energy NMR structure (gray) with Frq1 (1FPW; NMR, cyan[6]), human NCS-1 (1G8I; X-ray, red[7]), and Frq1/Pik1$^{121–174}$ (2JU0; NMR, blue[15]). Only backbone atoms from helical regions were used for the alignment. L2 and L3 have been omitted for clarity. (b) The HC (blue) and L3 (green) in all Ca^{2+}-loaded NCS-1 structures: human NCS-1 NMR solution structure (top left), NMR structure of the Pik1–Frq1 complex (2JU0; top right), X-ray structure of human NCS-1 (1G8I; bottom left), and NMR structure of yeast Frq1 (1FPW; bottom right). The Pik1 fragment in 2JU0 and the ethylene glycol molecules in 1G8I are shown in red cartoon and space-filled atoms, respectively.

Table 2. Comparison of different NCS-1 structures using Modeller 6.1

	2LCP	1FPW	2JU0 (bound)
1FPW	79.8%[a] (1.99 Å[b])	—	
2JU0 (bound)	74.1% (2.22 Å)	77.2% (2.02 Å)	
1G8I	71.5% (2.00 Å)	75.1% (1.86 Å)	81.9% (1.81 Å)

[a] The percentage of C^{α} atoms within 2 Å.
[b] RMSDs of C^{α} atoms superimposed.

adjuvants in the HC of NCS-1 (Fig. 2b). The two structures align with 82% of their C^{α} atoms within an RMSD of 1.8 Å (Table 2). Moreover, a low identity between the two sets of NOEs was observed, suggesting that either recoverin is not an optimal model for NCS-1 or different sample conditions may change the conformation of NCS-1. Compared to the human NCS-1 structure, a sizeable conformational shift is notable in helices H2, H3, and H5 in the crystal structure and in the Pik1$^{121–174}$/Frq1 complex structure (Fig. 2a). This is addressed further in the Discussion. The L3 and the HC of the four structures are compared in Fig. 2b. The L3 of the NMR structure of human NCS-1 is bound within the HC (Fig. 2b, top left), stretching in some cases through to the N-domain (Fig. 1c). The NMR structure of yeast Frq1 also has L3 within the HC, but with an α-helical secondary structure (Fig. 2b, bottom right), leaving a large hydrophobic patch exposed to the solvent. In contrast, the crystal structure has, as mentioned, adjuvant molecules in the HC, and here L3 forms a helix on the edge of the crevice (Fig. 2b, bottom left). The structure of the Pik1$^{121–174}$/NCS-1 complex shows that the Pik1 peptide covers the HC but does not resolve the orientation of the L3 segment (Fig. 2b, top right).

L3 is crucial for conformational stability in the Ca^{2+}-activated state

To test the significance of the L3 tail for structural integrity and stability in NCS-1, we designed a variant in which the last 15 C-terminal residues were removed (NCS-1$^{\Delta 176–190}$). A far-UV circular dichroism (CD) spectrum of this variant was closely similar to that of wt-NCS-1, indicating that the secondary structure content is overall maintained (Fig. 3a). We then followed the global guanidine hydrochloride (GuHCl)-induced unfolding of wt-NCS-1 and NCS-1$^{\Delta 176–190}$ by monitoring changes in intrinsic fluorescence intensity (Fig. 3b). As shown previously,[8,27] two major unfolding transitions were observed in the wild type, presumably reflecting the sequential unfolding of each structural domain. The transitions were fitted to $\Delta G_{N–D}^{H_2O}(1) = -35.1 \pm 4.4$ kJ mol^{-1} and $\Delta G_{N–D}^{H_2O}(2) = -38.2 \pm 8.3$ kJ mol^{-1}, suggesting equal stability of the two domains under these conditions (Table 3). Unfolding of NCS-1$^{\Delta 176–190}$ exhibited similar cooperative unfolding transitions

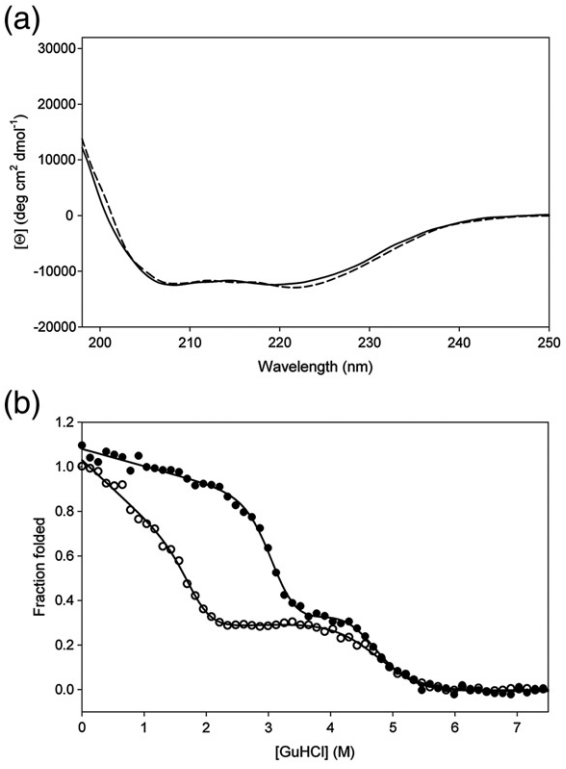

Fig. 3. Characterization of the global stability and secondary structure of the NCS-1$^{\Delta 176–190}$ variant. (a) Far-UV CD spectra of wt-NCS-1 (continuous line) and NCS-1$^{\Delta 176–190}$ (broken line). The protein concentration was 15 μM, and the light path length was 1 mm. (b) GuHCl-induced unfolding profile of wt-NCS-1 (filled circles) and NCS-1$^{\Delta 176–190}$ (empty circles), monitored by fluorescence emission intensity at 325 nm with excitation at 295 nm, at room temperature. The continuous lines represent the best fit to the data using Eq. (3).

indicative of a globular folded protein with two domains. Still, the first major transition was severely destabilized with a $\Delta\Delta G_{N–D}{}^{H_2O}(1)$ of −15.4 ± 3.2 kJ mol^{-1}, while the second was not significantly affected with a $\Delta\Delta G_{N–D}{}^{H_2O}(2)$ of 0.89 ± 1.04 kJ mol^{-1} (Fig. 3). To determine the origin of the different transitions, we engineered two additional variants of NCS-1 in which each of the two tryptophans W30 and W103, practically located with one in each domain, was substituted with a phenylalanine of low-fluorescence quantum yield. Equilibrium unfolding of these two variants pinpointed to the first major transition to the N-domain of NCS-1, and the second one pinpointed to the C-domain (Fig. 4). Hence, L3, despite being positioned most distal to the N-domain, has a significant stabilizing effect on the structural integrity of this domain and of the binding crevice.

Contrary to the $^{1}H,^{15}N$ HSQC spectrum of wt-NCS-1, the spectrum of the deletion variant NCS-1$^{\Delta 176–190}$ revealed a severe signal broadening of the entire protein, indicative of a highly heterogeneous conformational ensemble (Fig. 5a and b). However, the cooperative unfolding transitions observed in the equilibrium unfolding experiments rule out that a molten globule state is the origin of the collapsed NMR spectrum. Furthermore, the NMR samples were transparent, with no visual signs of aggregation. We therefore attempted to reestablish the conformational integrity of NCS-1$^{\Delta 176–190}$ by titrating in a peptide corresponding to the tail residues D176-V190 while following $^{1}H,^{15}N$ chemical shifts of NCS-1$^{\Delta 176–190}$ (Fig. 5c). The peptide reestablished the chemical shift dispersion of a narrow structure ensemble, suggesting that the peptide bound to NCS-1. A total of 134 out of a possible 159 (~85%) resonance signals reappeared at large peptide excess (12:1). The ^{1}H and ^{15}N chemical shifts were combined according to the equation described in Materials and Methods and compared to wt-NCS-1. Significant chemical shift differences were observed as expected due to the release of L3 from NCS-1. The three signature peaks at high field that correspond to the glycines in each calcium binding EF-hand loop reappeared, and many residues of the crevice were not perturbed, suggesting that the L3 peptide was bound in the same binding site as in the intact protein. A plot of the chemical shift difference between wt-NCS-1 and the variant in complex with the L3 peptide revealed that the more severe perturbations were found mostly in the C-domain (Fig. 5d). Residues displaying perturbations of more than 1 SD from the mean were Y31, I35, G41, A88, S90, V91, S93, and G95 in the N-domain,

Table 3. Thermodynamic parameters of the unfolding of NCS-1 and variants

	N-domain				C-domain			
	m (kJ mol^{-1} M^{-1})	C_m (M)	$\Delta G_{N–D}$ (kJ mol^{-1})	$\Delta\Delta G_{N–D}$ (kJ mol^{-1})[a]	m (kJ mol^{-1} M^{-1})	C_m (M)	$\Delta G_{N–D}$ (kJ mol^{-1})	$\Delta\Delta G_{N–D}$ (kJ mol^{-1})
Wild type	11.3 ± 1.4	3.11 ± 0.07	−35.1 ± 4.4	—	8.3 ± 1.8	4.61 ± 0.2	−38.2 ± 8.3	—
Δ176–190	12.7 ± 2.0	1.82 ± 0.04	−23.1 ± 3.8	−15.4 ± 3.2	6.5 ± 0.9	4.73 ± 0.07	−30.8 ± 4.5	0.89 ± 1.04
W30F	—	—	—	—	7.3 ± 0.5	4.99 ± 0.03	−36.2 ± 2.5	2.96 ± 0.96
W103F	11.9 ± 0.7	3.17 ± 0.01	−37.8 ± 2.2	0.70 ± 0.47	—	—	—	—
R102Q	12.2 ± 2.4	3.07 ± 0.12	−37.5 ± 7.4	−0.47 ± 1.1	7.6 ± 1.8	4.44 ± 0.25	−33.8 ± 8.3	−1.35 ± 1.77

[a] $\Delta\Delta G_{N–D}$ calculated as $m_{avg}\Delta C_m$.

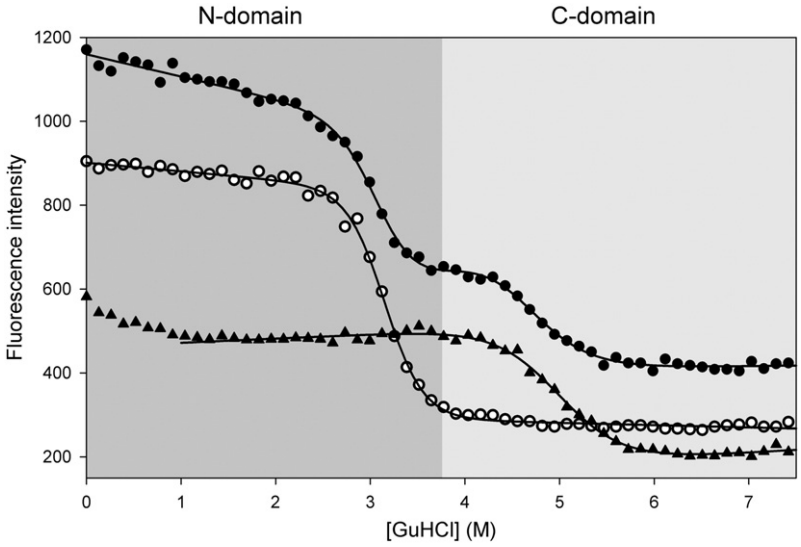

Fig. 4. Comparison of GuHCl unfolding profiles for the assignment of unfolding transitions to structural regions. The unfolding transitions of wt-NCS-1 (filled circles), NCS-1^{W103F} (empty circles), and NCS-1^{W30F} (triangles) are shown. The continuous lines represent the best fit to the data using Eq. (3) for wt-NCS-1 and Eq. (2) for the mutants. The first 11 data points for NCS-1^{W30F} were excluded from the fit.

and F105, L107, L110, T117, M121, G133, E140, E141, E142, K158, L166, and Q170 in the C-domain. Residues A88, S90, V91, S93, and G95 can be considered to be on the interface of the two domains, and residues A88, V91, F105, L110, and M121 contribute to the HC.

R102Q mutation has long-range chemical shift effects on L3 and HC

Recently, a single mutation in human NCS-1, substituting R102 for glutamine (R102Q), was discovered in a patient suffering from autistic spectrum disorder.[28] It has already been demonstrated that this variant has structural and functional deficits, most notably a loss of the Ca^{2+}-dependent component of plasma membrane cycling.[29] To examine whether local or global structure or stability was altered in this variant, we compared the changes in stability toward chemical denaturation and the changes in backbone chemical shifts to those of wt-NCS-1.

First, we followed GuHCl-induced unfolding by monitoring changes in intrinsic fluorescence intensity, as described above. The NCS-1^{R102Q} variant was only slightly destabilized with respect to the wild type, minimally affecting the second major unfolding transition corresponding to the unfolding of the C-domain, an observation fully in line with the position of the mutation site (Fig. 6a, Table 3).

Next, to determine any structural differences on a residue-specific basis, we measured and analyzed the $^{1}H,^{15}N$ HSQC spectra of both wt-NCS-1 and NCS-1^{R102Q} (Fig. S2) and plotted the difference in chemical shifts, as described above (Fig. 6b). The trimmed average chemical shift difference (15% of the highest shift differences not included in the calculated average) was 0.024 ± 0.012 ppm. The most prominent chemical shift changes, including those displaying more than 1 SD from the average, were evenly distributed in both domains. Residues with severe chemical shift perturbations were located distinctly around the mutation site in H6 and H9 and in L3, but also in the N-domain. The most perturbed residues were mapped onto the structure of NCS-1 (Fig. 6c). Many residues that form the HC, including Y52, V68, F69, and F85 in the N-domain, and W103 and L110 in the C-domain, were severely perturbed. In addition, residues I179, V180, L183, and Y186, all of which are located in L3, were perturbed beyond 1 SD from average.

Lastly, we examined if the R102Q substitution had any effect on the fast timescale dynamics of the protein and recorded the transverse R_2 ^{15}N relaxation rates of wt-NCS-1 and NCS-1^{R102Q} (Fig. S3). For each structural element, we calculated an average R_2 value, $\langle R_2 \rangle$, and correlated these values between wild type and mutant (Fig. 6d). There was a good correlation between the two ($R^2 = 0.87$; $R = 0.93$), except for the L3 segments, which had distinctly lower $\langle R_2 \rangle$ values in the R102 mutant. This suggests that L3 has dampened mobility in NCS-1^{R102Q}, indicating that a possible contribution from chemical exchange had vanished here. Moreover, we note that the global average value $\langle R_2 \rangle_{global}$, which relates to the overall tumbling of the molecule, is higher in wt-NCS-1 (16.8 s^{-1} *versus* 14.9 s^{-1}), consistent with a more compact mutant protein.

Discussion

We have determined the solution structure of Ca^{2+}-bound unmyristoylated human NCS-1 and have

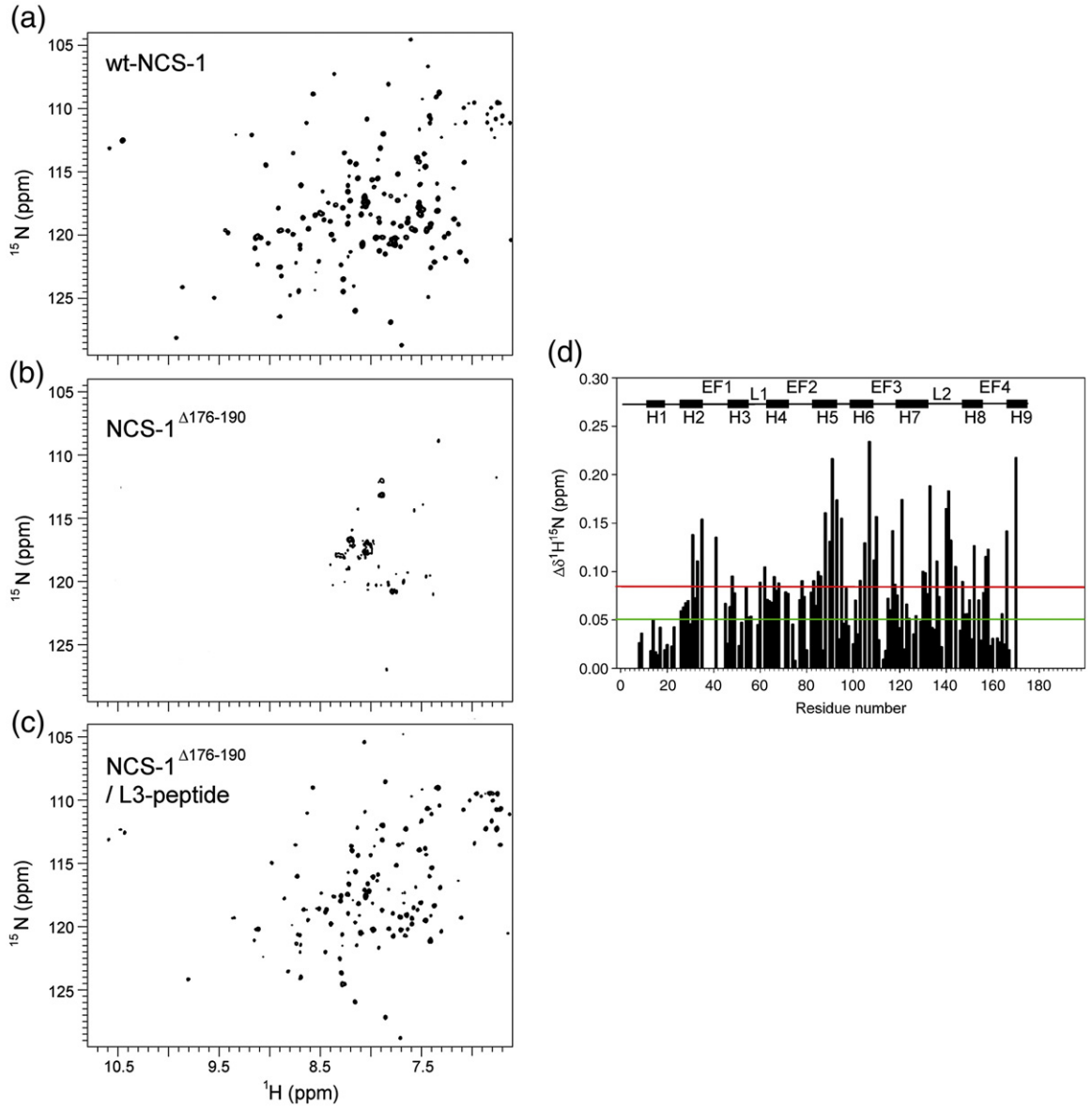

Fig. 5. L3–peptide binding to the HC of human NCS-1. (a) $^{1}H,^{15}N$ HSQC spectra of wt-NCS-1, (b) NCS-1$^{\Delta 176–190}$, and (c) NCS-1$^{\Delta 176–190}$ in complex with the L3–peptide (bottom). (d) Combined $^{1}H,^{15}N$ chemical shift differences between wt-NCS-1 and the NCS-1$^{\Delta 176–190}$ variant plotted as a function of residue number. The green and red lines denote the average and 1 SD, respectively. The positions of helices, loops, and EF hands are indicated.

focused on the structural features of the HC and the C-terminal tail. We observed that the C-terminal segment (L3) of NCS-1 is situated in the HC, where it may act as a ligand mimic in the absence of an interaction partner, as well as an integrator of the conformational stability of NCS-1.

Overall, the structure of human NCS-1 is similar to the NMR/homology model of yeast Frq1. However, in addition to the observation of significant domain movements upon ligand binding (Fig. 2a), there are striking differences in the orientation and shape of L3 and the HC. A number of NOEs between L3 and residues from helices H6–H8 suggested L3 to be positioned within the HC, and this location was supported by drastic global destabilization by tail truncation. Additionally, the severe destabilization of the N-domain upon tail truncation indicates that the tail may transiently interact with that domain, despite a lack of NOEs. The chemical shift differences between the wild type and the tail truncation variant indicated further that the peptide binds in the C-domain, as shift perturbations were located mostly at helical ends and at the domain interface more than in the HC, but

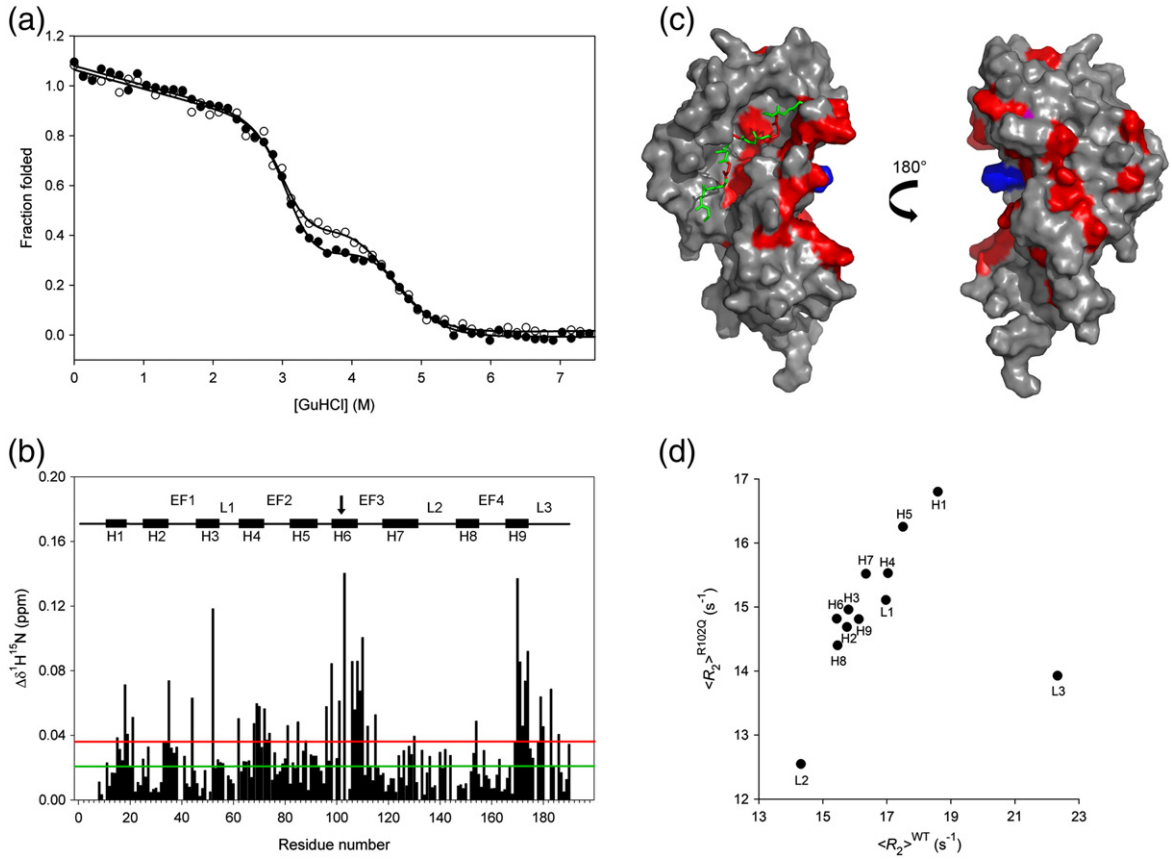

Fig. 6. Characterization of the global stability and structure of the NCS-1^{R102Q} variant. (a) GuHCl-induced unfolding of wt-NCS-1 (filled circles) and NCS-1^{R102Q} (empty circles), monitored by fluorescence intensity at 325 nm with excitation at 295 nm, at room temperature. The continuous lines represent the best fit to the data using Eq. (3). (b) Combined ^{1}H,^{15}N chemical shift differences between wt-NCS-1 and NCS-1^{R102Q} plotted as a function of residue number. The green and red lines denote the average and 1 SD, respectively. The positions of helices, loops, and EF hands are indicated, and the site of mutation is shown by an arrow. (c) Residues with large perturbations were mapped onto the structure of wt-NCS-1. Residues that were perturbed by more than 1 SD are shown in red. The R102 side chain is shown in blue. (d) Correlation between the transverse ^{15}N relaxation rates for each structural segment in NCS-1 and NCS-1^{R102Q}. Each segment is labeled according to either helix (H) or loop (L).

also some perturbations were observed in the N-domain. Lastly, in support of our conclusion, the structure of the N-domain of the yeast Frq1 N-domain apparently was inaccessible, and NOEs from recoverin were applied to model this part of the structure. Retrospectively, this construct has a C-terminal His_6-tag, and this could, by analogy, lead to domain destabilization. Instead, the orientation of the tail that we observe in human NCS-1 is similar to that seen in KchIP1 (*Kv channel interacting protein 1*), a fellow member of the NCS family,[30] and to that seen in CIB1 (*calcium and integrin binding protein 1*), a protein that shares significant sequence homology with NCS-1.[31] In CIB1, the tail binds weakly to the HC and is displaced when the protein encounters a binding partner; in KchIP1, a tail truncation variant was shown to no longer modulate expression levels of Kv4.2 proteins. The drastic conformational destabilization upon deletion of the tail has so far only been described for NCS-1 but may possibly be universal in the entire family of NCS proteins. This remains to be established.

These results stand in marked contrast to the conformation of L3 described from the structures previously available. From the structural alignment in Fig. 2a, a conformational shift in helices H1, H2, H3, and H5 is observed between the set of structures, depending on occupation by ligand or tail in the HC. Thus, an apparent flexibility of the helices in the N-domain of NCS-1 may be important for a spacious accommodation in the HC of the wide array of ligands that interact with NCS-1. The NCS family has a suggested plethora of interaction partners, and the nature of most of these interactions is not clear. However, it can be expected that these interact with NCS-1 through an amphipathic—most likely helical—motif.[14,16,17] L3 in human NCS-1 is without stable secondary structure, but it may well

be that it forms a transient α-helical structure. In fact, when the ensemble of the 20 lowest-energy structures is inspected, the first part of L3 forms, in some of the structures, what may indeed be interpreted as an α-helical structure. It is therefore possible that L3 changes between an unstructured loop (which allows it to stretch into the N-domain, stabilizing the integrity of the crevice and the globular fold) and a transient helical structure similar to what is formed in the complex. Moreover, the hydrophobic pattern of L3 similar to the amphipathic nature of the abovementioned interaction partners suggests that, besides contributing to domain integrity, its role as a ligand mimetic may also be suggested.

The myristoyl group has been suggested to act as a folding chaperone for NCS proteins until they reach the membrane.[32] This, together with the suggestion that NCS-1 is constitutively membrane bound and thus leaves the myristoyl group occupied in the membrane,[10] is interesting, but this model demands for a protective shield of the HC in the membrane environment until ligand interactions are needed. Such a role may be fulfilled by L3. In an activated Ca^{2+}-bound NCS-1 and in the absence of ligand, we suggest that the C-terminal tail (L3) take on the transient role of a ligand and that the myristoyl group constitutively interact with the membrane. The model is illustrated in Fig. 7. Thus, in case of observed activity loss for unmyristoylated NCS-1, this may indeed be linked to defective localization and hence indirectly to the availability of the myristoyl group. Since no structural data on the unmyristoylated human NCS-1 are available, this state is omitted from the model. For the same reasons, conformational changes associated with the calcium-sensing site EF4 are not included.

We observed domain autonomy in NCS-1 with individual unfolding transitions for each domain, but with distinct structural cross-talk between them. One clue to the reason for these observations comes from the analyses of the NCS-1^{R102Q} variant, for which malfunctions have been reported.[29] We observed that this mutation not only affected the local environment but also changed the chemical shifts and, more distinctly, the dynamics of the L3 segment distal to the mutation site. The dynamic change in L3 leaves the possibility that interactions with the HC may be compromised in the variant, which could then lead to an altered equilibrium between the L3-bound state and the L3-unbound state and to local unfolding or collapse of the interdomain cross-talk. In the NCS-1^{R102Q} variant, V180 and L183 of L3 have large chemical shift changes, suggesting that the HC is either more exposed to water or more occupied by L3. From the decreased average R_2 value of the NCS-1^{R102Q} variant, the latter seems to be more likely. Of particular interest is that the chemical shifts of Y52 and F85 were affected significantly in the NCS-1^{R102Q} variant. These residues belong to the N-domain and support the notion that L3 may reach this far into the N-domain, making contacts with Y52 and F85 in the wild type but being absent in the variant (or *vice versa*). The extent to which the mutation affects the binding profile of NCS-1 is also not known from the present data. It has been shown *in vitro* that the NCS-1^{R102Q} variant does not have an altered binding affinity for IL1RAPL1 (*IL-1 r*eceptor *a*ccessory *p*rotein *l*ike *1*), which has been associated with autistic spectrum disorder.[28,29] The mutation does, however, cause altered cycling in the plasma membrane with a loss of Ca^{2+} dependency. Whether the myristoyl group is trapped in the HC of the NCS-1^{R102Q} variant because of altered L3 occupancy in the HC is unknown but may explain why it has lost its Ca^{2+}-dependent component in membrane cycling.

It is well known that the HC of neuronal calcium sensors can bind specific target proteins from a broad spectrum of partners. However, to the best of our knowledge, this is the first study to provide

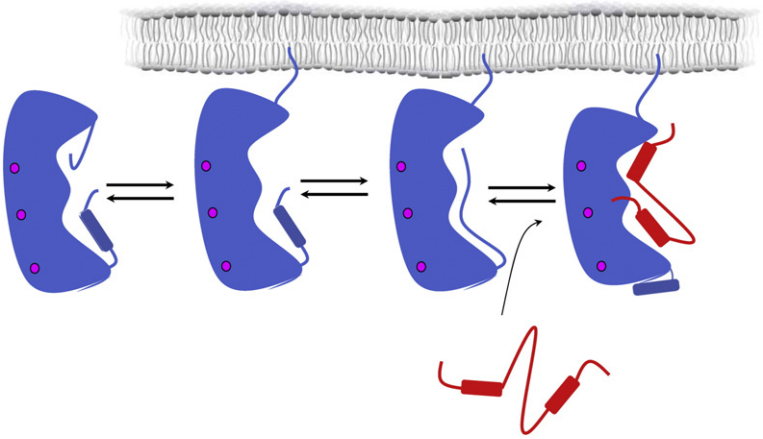

Fig. 7. The C-terminal tail L3 may act as a ligand mimic at activating levels of Ca^{2+}. Before membrane attachment, myristoyl acts as a folding chaperone (right). When inserted into the membrane and in the absence of a ligand, L3 takes the role of a transient ligand to protect the HC and to stabilize the structural integrity of NCS-1. The model assumes a constitutive membrane association of Ca^{2+}-loaded NCS-1. Since there are no available experimental data on the unmyristoylated human NCS-1 or on conformational changes associated with the calcium-sensing site EF4, these states are omitted from the model.

atomic-level experimental evidence for the possibility of the C-terminal segment (L3) being bound in the HC, which is crucial to the global conformational stability of the Ca^{2+}-activated state. Since the integrity of NCS-1 is dependent on L3 and since the amphipathic nature of L3 mimics those of the known ligands, we propose a model describing how NCS-1 may respond to interactions with other molecules (Fig. 7). This model suggests that the degree of opening or closing of the HC may be controlled by cellular fluctuations of calcium and/or magnesium concentration, as well as by exchange of L3 from the crevice. The extent of flexibility of the individual structural parts of NCS-1 and the importance of interdomain cross-talk for stability and ligand binding selectivity still remain to be determined. How such parameters and tail occupancy in the HC and an accompanying conformational stabilization will affect or even control ligand binding to calcium sensors remain to be fully explored.

Materials and Methods

Protein expression and purification

Recombinant unmyristoylated human NCS-1 uniformly labeled with ^{15}N was expressed from the pET-16b vector in *Escherichia coli* strain BL21(DE3). It was grown at 37 °C in M9 minimal medium containing $^{15}NH_4SO_4$ as the sole source for nitrogen. The protein was purified as described previously,[22] but using protamine sulfate instead of streptomycin sulfate. ^{15}N,^{13}C-labeled proteins were obtained by growing the bacteria in M9 minimal medium containing $^{15}NH_4SO_4$ as the sole source for nitrogen and [$^{13}C_6$]glucose as the sole source for carbon. The variants NCS-$1^{\Delta 176–190}$ and NCS-1^{R102Q} were generated from the wild-type plasmid using oligonucleotide primers containing the respective mutations and the QuikChange Lightning ® site-directed mutagenesis kit. The peptide corresponding to amino acid residues D176-V190 was purchased in N-terminal acetylated form from Schafer-N (Copenhagen, Denmark).

NMR spectroscopy

The following NMR spectra were recorded on a Varian UNITY*plus* 600-MHz spectrometer (1.4 mM protein concentration at pH 7.2, 8 mM $CaCl_2$, and 14 mM DTT at 37 °C): two-dimensional (2D) ^{15}N,^{1}H HSQC, 3D ^{15}N TOCSY-HSQC, 3D ^{15}N NOESY-HSQC, 3D ^{13}C NOESY-HSQC, 3D HNCA, 3D HNCO, 3D HN(CO)CA, 3D CBCA(CO)HN, 3D CBCACOHA, 3D HCCH-TOCSY, and four-dimensional ^{13}C NOESY-HSQC.[33–38] Amide hydrogen exchange in NCS-1 was evaluated by a comparison of 2D ^{15}N,^{1}H HSQC recorded in 10% (vol/vol) D_2O and that recorded in 99.96% (vol/vol) D_2O after 12 h and 24 h of exchange. All spectra were processed using MNMR[39] or NMRPipe.[40] ^{1}H chemical shifts were referenced to the methyl proton resonances of an external DSS standard at 0.00 ppm, and ^{15}N and ^{13}C chemical shifts were indirectly referenced as described previously.[41] In addition, the following spectra were recorded using a Varian UNITY 800-MHz spectrometer with z-gradients (0.8 mM protein concentration at pH 7.2, 10 mM Tris–HCl, 10 mM $CaCl_2$, and 2 mM TCEP–HCl): 2D ^{1}H,^{15}N HSQC, 3D HCCH-TOCSY in the aromatic area, and 3D ^{13}C NOESY-HSQC in both the aromatic area and the aliphatic area.[42,43] For assignment of aromatic side-chain resonances, we recorded at a set of 2D HBCBCGCDCDHE and HBCBCGCDHD correlation spectra as described previously,[44] with the number of increments 2048 in the direct dimension. To aid in defining the extent of the helical structures, we measured $^{3}J_{HN–H\alpha}$ coupling constants with water flip-back J-resolved CT-HMQC experiments.[45]

The peptide corresponding to the L3 tail residues D176-V190 was titrated into a sample containing 50 μM NCS-$1^{\Delta 176–190}$, 10 mM Tris, 5 mM $CaCl_2$ (pH 7.2), 2 mM DTT, 10% D_2O, and 0.02% NaN_3 at 37 °C. ^{1}H,^{15}N HSQCs were recorded at 37 °C using samples with varying concentrations of peptide in the range 100–600 μM.

The ^{15}N R_2 relaxation spectra of ^{15}N-labeled NCS-1 or NCS-1^{R102Q} [0.6 mM NCS-1, 10 mM $CaCl_2$, and 6 mM DTT (pH 7.2)] were recorded at 310 K with 256 and 2048 data points in t_1 and t_2. The spectral widths were 3200 Hz in t_1 and 12,000 Hz in t_2. Of each sample, an array of 12 ^{15}N R_2 spectra was recorded, with delay times of 10 ms, 30 ms, 50 ms, 70 ms, 90 ms, 110 ms, 150 ms, 170 ms, 210 ms, and 250 ms. Each array of spectra was recorded interleaved.

Assignment and structure calculation

Sequential and side-chain assignments were performed manually using Pronto3D.[39] All NOEs were manually assigned, with a final result of 1298 signals with useful distance information. The experimentally determined distance restraints were sorted in DIANA and, together with dihedral-angle restraints determined by TALOS,[23] used in structure calculations with a standard protocol of Xplor-NIH,[46,47] including a conformational database potential.[48] A total of six Ca^{2+}–ligand distance constraints per Ca^{2+} binding loop were incorporated, with the lower bound set to 2.0 Å in all cases.[24] After iterative rounds of refinements, a final total of 100 structures were calculated, 20 structures with fulfilled experimental constraints and the lowest energy were selected, and structural quality was evaluated using PROCHECK-NMR.[49,50]

Assignment of ^{1}H and ^{15}N resonance signals in NCS-1^{R102Q} and NCS-$1^{\Delta 176–190}$ could be accomplished directly by the transfer of the 174 peaks assigned in the wild type. Chemical shift differences between wild-type NCS-1 and NCS-1^{R102Q} were calculated with Eq. (1):[51]

$$\Delta\delta(\text{ppm}) = \sqrt{\Delta\delta\left(^{1}\text{H}\right)^2 + 0.154\Delta\delta\left(^{15}\text{N}\right)^2} \qquad (1)$$

Determination of protein stability

GuHCl denaturation of wild-type NCS-1, NCS-$1^{\Delta 176–190}$, and NCS-1^{R102Q} was monitored by intrinsic fluorescence emission spectroscopy using a Perkin-Elmer LS50B. Samples of 15 μM protein were prepared in 20 mM

Tris, 5 mM $CaCl_2$, and 2 mM DTT (pH 7.2), with GuHCl concentrations in the range 0–6.5 M. The exact denaturant concentration was determined with a digital refractometer. All experiments were performed at ambient temperatures, with excitation at 295 nm monitoring emission at 325 nm. Emission spectra were averaged over three scans. The fraction of folded protein was calculated from the maximum and minimum intensities, and plotted against the concentration of denaturant. The data were fitted to either two-state transitions using Eq. (2) or three-state transitions using Eq. (3), as described previously.[52] At least 60 data points were used in each experiment:

$$f(x) = \frac{(a_0 + a_1 x) + (a_2 + a_3 x)\exp(m(x - C_m)/RT)}{1 + \exp(m(x - C_m)/RT)} \quad (2)$$

$$f(x) = \frac{(a_0 + a_1 x) + (a_2 + a_3 x)\exp(m_1(x - C_{m1})/RT)}{1 + \exp(m_1(x - C_{m1})/RT)} + \frac{(a_2 + a_3 x) + (a_4 + a_5 x)\exp(m_2(x - C_{m2})/RT)}{1 + \exp(m_2(x - C_{m2})/RT)} \quad (3)$$

where a_0, a_1, a_2, a_3, a_4, and a_5 are the linear influences of denaturant on the different states N, $[D_N N_C]$, and D, respectively. The conformational stability for the different states was calculated as $\Delta G^{H_2O}_{N-D} = -|m|C_m$.

CD spectroscopy

Far-UV CD spectra were measured from 250 nm to 190 nm on a Jasco J-810 spectropolarimeter on 15 μM protein samples at 37 °C in 20 mM Tris and 5 mM $CaCl_2$ (pH 7.2), accumulating five spectra and subtracting buffer background. The light path length was 1 mm.

Accession number

Structure coordinates have been deposited in the Protein Data Bank under accession code 2LCP. Assigned backbone resonances have been previously deposited in the Biological Magnetic Resonance Bank under accession code 4378.

Acknowledgements

This work was supported by the Carlsberg Foundation and The Danish Council for Independent Research | Natural Sciences (B.B.K.) and the Swedish Foundation for Strategic Research (B.E.F.). We thank the Knut and Alice Wallenberg Foundation for generously providing funds for the purchase of the Varian UNITY*plus* 600-MHz spectrometer in Lund and The John and Birthe Meyer Foundation for the establishment of SBiNLab.

Supplementary Data

Supplementary data to this article can be found online at doi:10.1016/j.jmb.2011.12.049

References

1. Rivosecchi, R., Pongs, O., Theil, T. & Mallart, A. (1994). Implication of frequenin in the facilitation of transmitter release in *Drosophila*. *J. Physiol.* **474**, 223–232.
2. Tsujimoto, T., Jeromin, A., Saitoh, N., Roder, J. C. & Takahashi, T. (2002). Neuronal calcium sensor 1 and activity-dependent facilitation of P/Q-type calcium currents at presynaptic nerve terminals. *Science*, **295**, 2276–2279.
3. Pongs, O., Lindemeier, J., Zhu, X. R., Theil, T., Engelkamp, D., Krah-Jentgens, I. *et al.* (1993). Frequenin—a novel calcium-binding protein that modulates synaptic efficacy in the *Drosophila* nervous system. *Neuron*, **11**, 15–28.
4. Burgoyne, R. D. & Weiss, J. L. (2001). The neuronal calcium sensor family of Ca^{2+}-binding proteins. *Biochem. J.* **353**, 1–12.
5. Gifford, J. L., Walsh, M. P. & Vogel, H. J. (2007). Structures and metal-ion-binding properties of the Ca^{2+}-binding helix–loop–helix EF-hand motifs. *Biochem. J.* **405**, 199–221.
6. Ames, J. B., Hendricks, K. B., Strahl, T., Huttner, I. G., Hamasaki, N. & Thorner, J. (2000). Structure and calcium-binding properties of Frq1, a novel calcium sensor in the yeast *Saccharomyces cerevisiae*. *Biochemistry*, **39**, 12149–12161.
7. Bourne, Y., Dannenberg, J., Pollmann, V., Marchot, P. & Pongs, O. (2001). Immunocytochemical localization and crystal structure of human frequenin (neuronal calcium sensor 1). *J. Biol. Chem.* **276**, 11949–11955.
8. Aravind, P., Chandra, K., Reddy, P. P., Jeromin, A., Chary, K. V. & Sharma, Y. (2008). Regulatory and structural EF-hand motifs of neuronal calcium sensor-1: Mg^{2+} modulates Ca^{2+} binding, Ca^{2+}-induced conformational changes, and equilibrium unfolding transitions. *J. Mol. Biol.* **376**, 1100–1115.
9. Lim, S., Strahl, T., Thorner, J. & Ames, J. B. (2011). Structure of a Ca^{2+}–myristoyl switch protein that controls activation of a phosphatidylinositol 4-kinase in fission yeast. *J. Biol. Chem.* **286**, 12565–12577.
10. McFerran, B. W., Weiss, J. L. & Burgoyne, R. D. (1999). Neuronal Ca(2+) sensor 1. Characterization of the myristoylated protein, its cellular effects in permeabilized adrenal chromaffin cells, Ca(2+)-independent membrane association, and interaction with binding proteins, suggesting a role in rapid Ca(2+) signal transduction. *J. Biol. Chem.* **274**, 30258–30265.
11. Zozulya, S. & Stryer, L. (1992). Calcium–myristoyl protein switch. *Proc. Natl. Acad. Sci. USA*, **89**, 11569–11573.
12. O'Callaghan, D. W. & Burgoyne, R. D. (2004). Identification of residues that determine the absence of a Ca(2+)/myristoyl switch in neuronal calcium sensor-1. *J. Biol. Chem.* **279**, 14347–14354.
13. Strahl, T., Grafelmann, B., Dannenberg, J., Thorner, J. & Pongs, O. (2003). Conservation of regulatory function in calcium-binding proteins: human frequenin (neuronal calcium sensor-1) associates productively with yeast phosphatidylinositol 4-kinase isoform, Pik1. *J. Biol. Chem.* **278**, 49589–49599.
14. Hendricks, K. B., Wang, B. Q., Schnieders, E. A. & Thorner, J. (1999). Yeast homologue of neuronal frequenin is a regulator of phosphatidylinositol-4-OH kinase. *Nat. Cell Biol.* **1**, 234–241.

15. Strahl, T., Huttner, I. G., Lusin, J. D., Osawa, M., King, D., Thorner, J. & Ames, J. B. (2007). Structural insights into activation of phosphatidylinositol 4-kinase (Pik1) by yeast frequenin (Frq1). *J. Biol. Chem.* **282**, 30949–30959.
16. Sallese, M., Iacovelli, L., Cumashi, A., Capobianco, L., Cuomo, L. & De Blasi, A. (2000). Regulation of G protein-coupled receptor kinase subtypes by calcium sensor proteins. *Biochim. Biophys. Acta*, **1498**, 112–121.
17. Kabbani, N., Negyessy, L., Lin, R., Goldman-Rakic, P. & Levenson, R. (2002). Interaction with neuronal calcium sensor NCS-1 mediates desensitization of the D2 dopamine receptor. *J. Neurosci.* **22**, 8476–8486.
18. Nakamura, T. Y., Sturm, E., Pountney, D. J., Orenzoff, B., Artman, M. & Coetzee, W. A. (2003). Developmental expression of NCS-1 (frequenin), a regulator of Kv4 K^+ channels, in mouse heart. *Pediatr. Res.* **53**, 554–557.
19. Bahi, N., Friocourt, G., Carrie, A., Graham, M. E., Weiss, J. L., Chafey, P. *et al.* (2003). IL1 receptor accessory protein like, a protein involved in X-linked mental retardation, interacts with neuronal calcium sensor-1 and regulates exocytosis. *Hum. Mol. Genet.* **12**, 1415–1425.
20. Schaad, N. C., De Castro, E., Nef, S., Hegi, S., Hinrichsen, R., Martone, M. E. *et al.* (1996). Direct modulation of calmodulin targets by the neuronal calcium sensor NCS-1. *Proc. Natl Acad. Sci. USA*, **93**, 9253–9258.
21. Yamniuk, A. P. & Vogel, H. J. (2004). Calmodulin's flexibility allows for promiscuity in its interactions with target proteins and peptides. *Mol. Biotechnol.* **27**, 33–57.
22. Kragelund, B. B., Hauenschild, A., Carlstrom, G., Pongs, O. & Finn, B. E. (2000). ^{1}H, ^{13}C, and ^{15}N assignments of un-myristoylated Ca^{2+}-frequenin, a synaptic efficacy modulator. *J. Biomol. NMR*, **16**, 85–86.
23. Cornilescu, G., Delaglio, F. & Bax, A. (1999). Protein backbone angle restraints from searching a database for chemical shift and sequence homology. *J. Biomol. NMR*, **13**, 289–302.
24. Atreya, H. S., Sahu, S. C., Bhattacharya, A., Chary, K. V. & Govil, G. (2001). NMR derived solution structure of an EF-hand calcium-binding protein from *Entamoeba histolytica*. *Biochemistry*, **40**, 14392–14403.
25. Schwieters, C. D., Kuszewski, J. J., Tjandra, N. & Clore, G. M. (2003). The Xplor-NIH NMR molecular structure determination package. *J. Magn. Reson.* **160**, 65–73.
26. Eswar, N., Webb, B., Marti-Renom, M. A., Madhusudhan, M. S., Eramian, D., Shen, M. Y. *et al.* (2006). Comparative protein structure modeling using Modeller. *Curr. Protoc. Bioinf.* Chapter 5, Unit 5.6.
27. Muralidhar, D., Jobby, M. K., Krishnan, K., Annapurna, V., Chary, K. V., Jeromin, A. & Sharma, Y. (2005). Equilibrium unfolding of neuronal calcium sensor-1: N-terminal myristoylation influences unfolding and reduces protein stiffening in the presence of calcium. *J. Biol. Chem.* **280**, 15569–15578.
28. Piton, A., Michaud, J. L., Peng, H., Aradhya, S., Gauthier, J., Mottron, L. *et al.* (2008). Mutations in the calcium-related gene IL1RAPL1 are associated with autism. *Hum. Mol. Genet.* **17**, 3965–3974.
29. Handley, M. T., Lian, L. Y., Haynes, L. P. & Burgoyne, R. D. (2011). Structural and functional deficits in a neuronal calcium sensor-1 mutant identified in a case of autistic spectrum disorder. *PLoS One*, **5**, e10534.
30. Zhou, W., Qian, Y., Kunjilwar, K., Pfaffinger, P. J. & Choe, S. (2004). Structural insights into the functional interaction of KChIP1 with Shal-type K(+) channels. *Neuron*, **41**, 573–586.
31. Yamniuk, A. P., Ishida, H. & Vogel, H. J. (2006). The interaction between calcium- and integrin-binding protein 1 and the alphaIIb integrin cytoplasmic domain involves a novel C-terminal displacement mechanism. *J. Biol. Chem.* **281**, 26455–26464.
32. Ames, J. B. & Lim, S. (2011). Molecular structure and target recognition of neuronal calcium sensor proteins. *Biochim. Biophys. Acta*,; E-publication ahead of print.
33. Grzesiek, S. & Bax, A. (1993). Amino acid type determination in the sequential assignment procedure of uniformly $^{13}C/^{15}N$-enriched proteins. *J. Biomol. NMR*, **3**, 185–204.
34. Vuister, G. W., Yamazaki, T., Torchia, D. A. & Bax, A. (1993). Measurement of two- and three-bond ^{13}C–^{1}H *J* couplings to the C delta carbons of leucine residues in staphylococcal nuclease. *J. Biomol. NMR*, **3**, 297–306.
35. Lee, W., Revington, M. J., Arrowsmith, C. & Kay, L. E. (1994). A pulsed field gradient isotope-filtered 3D ^{13}C HMQC-NOESY experiment for extracting intermolecular NOE contacts in molecular complexes. *FEBS Lett.* **350**, 87–90.
36. Feher, V. A., Zapf, J. W., Hoch, J. A., Dahlquist, F. W., Whiteley, J. M. & Cavanagh, J. (1995). ^{1}H, ^{15}N, and ^{13}C backbone chemical shift assignments, secondary structure, and magnesium-binding characteristics of the *Bacillus subtilis* response regulator, Spo0F, determined by heteronuclear high-resolution NMR. *Protein Sci.* **4**, 1801–1814.
37. Yamazaki, T., Nicholson, L. K., Torchia, D. A., Stahl, S. J., Kaufman, J. D., Wingfield, P. T. *et al.* (1994). Secondary structure and signal assignments of human-immunodeficiency-virus-1 protease complexed to a novel, structure-based inhibitor. *Eur. J. Biochem.* **219**, 707–712.
38. Zhang, H., Zhao, D., Revington, M., Lee, W., Jia, X., Arrowsmith, C. & Jardetzky, O. (1994). The solution structures of the trp repressor–operator DNA complex. *J. Mol. Biol.* **238**, 592–614.
39. Kjaer, M., Andersen, K. V. & Poulsen, F. M. (1994). Automated and semiautomated analysis of homo- and heteronuclear multidimensional nuclear magnetic resonance spectra of proteins: the program Pronto. *Methods Enzymol.* **239**, 288–307.
40. Delaglio, F., Grzesiek, S., Vuister, G. W., Zhu, G., Pfeifer, J. & Bax, A. (1995). NMRPipe: a multidimensional spectral processing system based on UNIX pipes. *J. Biomol. NMR*, **6**, 277–293.
41. Wishart, D. S., Bigam, C. G., Yao, J., Abildgaard, F., Dyson, H. J., Oldfield, E. *et al.* (1995). ^{1}H, ^{13}C and ^{15}N chemical shift referencing in biomolecular NMR. *J. Biomol. NMR*, **6**, 135–140.
42. Clore, G. M., Bax, A., Driscoll, P. C., Wingfield, P. T. & Gronenborn, A. M. (1990). Assignment of the side-chain ^{1}H and ^{13}C resonances of interleukin-1 beta using double- and triple-resonance heteronuclear three-dimensional NMR spectroscopy. *Biochemistry*, **29**, 8172–8184.
43. Kay, L. E., Clore, G. M., Bax, A. & Gronenborn, A. M. (1990). Four-dimensional heteronuclear triple-resonance NMR spectroscopy of interleukin-1 beta in solution. *Science*, **249**, 411–414.

44. Yamazaki, J. D., Forman-Kay, J. D. & Kay, L. E. (1993). 2D correlation of cb and hd, he of aromatic residues through JCC. *J. Am. Chem. Soc.* **115**, 11054.
45. Kuboniwa, H., Grzesiek, S., Delaglio, F. & Bax, A. (1994). Measurement of HN–H alpha *J* couplings in calcium-free calmodulin using new 2D and 3D water-flip-back methods. *J. Biomol. NMR*, **4**, 871–878.
46. Brunger, A. T., Clore, G. M., Gronenborn, A. M., Saffrich, R. & Nilges, M. (1993). Assessing the quality of solution nuclear magnetic resonance structures by complete cross-validation. *Science*, **261**, 328–331.
47. Brunger, A. T. & Nilges, M. (1993). Computational challenges for macromolecular structure determination by X-ray crystallography and solution NMR-spectroscopy. *Q. Rev. Biophys.* **26**, 49–125.
48. Kuszewski, J., Gronenborn, A. M. & Clore, G. M. (1997). Improvements and extensions in the conformational database potential for the refinement of NMR and X-ray structures of proteins and nucleic acids. *J. Magn. Reson.* **125**, 171–177.
49. Morris, A. L., MacArthur, M. W., Hutchinson, E. G. & Thornton, J. M. (1992). Stereochemical quality of protein structure coordinates. *Proteins*, **12**, 345–364.
50. Laskowski, R. A., Moss, D. S. & Thornton, J. M. (1993). Main-chain bond lengths and bond angles in protein structures. *J. Mol. Biol.* **231**, 1049–1067.
51. Ayed, A., Mulder, F. A., Yi, G. S., Lu, Y., Kay, L. E. & Arrowsmith, C. H. (2001). Latent and active p53 are identical in conformation. *Nat. Struct. Biol.* **8**, 756–760.
52. Maxwell, K. L., Wildes, D., Zarrine-Afsar, A., De Los Rios, M. A., Brown, A. G., Friel, C. T. *et al.* (2005). Protein folding: defining a "standard" set of experimental conditions and a preliminary kinetic data set of two-state proteins. *Protein Sci.* **14**, 602–616.